Neurobiology of Disease

Chronic Cortical Inflammation, Cognitive Impairment, and Immune Reactivity Associated with Diffuse Brain Injury Are Ameliorated by Forced Turnover of Microglia

Chelsea E. Bray,[1,3] Kristina G. Witcher,[1,3] Dunni Adekunle-Adegbite,[3] Michelle Ouvina,[3] Mollie Witzel,[3] Emma Hans,[3] Zoe M. Tapp,[1,3] Jonathan Packer,[1,3] Ethan Goodman,[1,3] Fangli Zhao,[1] Titikorn Chunchai,[4] Shane O'Neil,[1,3] Siriporn C. Chattipakorn,[4] John Sheridan,[1,3] Olga N. Kokiko-Cochran,[1,2,3] Candice Askwith,[1] and Jonathan P. Godbout[1,2,3]

[1]Department of Neuroscience, The Ohio State University, Columbus, Ohio 43210, [2]Chronic Brain Injury Program, The Ohio State University, Columbus, Ohio 43210, [3]Institute for Behavioral Medicine Research, The Ohio State University, Columbus, Ohio 43210, and [4]Neurophysiology unit, Cardiac Electrophysiology Research and Training Center, Faculty of Medicine, Chiang Mai University, Chiang Mai 50200, Thailand

Traumatic brain injury (TBI) is associated with an increased risk of cognitive, psychiatric, and neurodegenerative complications that may develop after injury. Increased microglial reactivity following TBI may underlie chronic neuroinflammation, neuropathology, and exaggerated responses to immune challenges. Therefore, the goal of this study was to force turnover of trauma-associated microglia that develop after diffuse TBI and determine whether this alleviated chronic inflammation, improved functional recovery and attenuated reduced immune reactivity to lipopolysaccharide (LPS) challenge. Male mice received a midline fluid percussion injury (mFPI) and 7 d later were subjected to a forced microglia turnover paradigm using CSF1R antagonism (PLX5622). At 30 d postinjury (dpi), cortical gene expression, dendritic complexity, myelin content, neuronal connectivity, cognition, and immune reactivity were assessed. Myriad neuropathology-related genes were increased 30 dpi in the cortex, and 90% of these gene changes were reversed by microglial turnover. Reduced neuronal connectivity was evident 30 dpi and these deficits were attenuated by microglial turnover. TBI-associated dendritic remodeling and myelin alterations, however, remained 30 dpi independent of microglial turnover. In assessments of functional recovery, increased depressive-like behavior, and cognitive impairment 30 dpi were ameliorated by microglia turnover. To investigate microglial priming and reactivity 30 dpi, mice were injected intraperitoneally with LPS. This immune challenge caused prolonged lethargy, sickness behavior, and microglial reactivity in the TBI mice. These extended complications with LPS in TBI mice were prevented by microglia turnover. Collectively, microglial turnover 7 dpi alleviated behavioral and cognitive impairments associated with microglial priming and immune reactivity 30 dpi.

Key words: brain injury; cognition; forced turnover; inflammation; lipopolysaccharide; microglia

Significance Statement

A striking feature of traumatic brain injury (TBI), even mild injuries, is that over 70% of individuals have long-term neuropsychiatric complications. Chronic inflammatory processes are implicated in the pathology of these complications and these issues can be exaggerated by immune challenge. Therefore, our goal was to force the turnover of microglia 7 d after TBI. This subacute 7 d postinjury (dpi) time point is a critical transitional period in the shift toward chronic inflammatory processes and microglia priming. This forced microglia turnover intervention in mice attenuated the deficits in behavior and cognition 30 dpi. Moreover, microglia priming and immune reactivity after TBI were also reduced with microglia turnover. Therefore, microglia represent therapeutic targets after TBI to reduce persistent neuroinflammation and improve recovery.

Received Sep. 20, 2021; revised Mar. 4, 2022; accepted Mar. 7, 2022.

Author contributions: C.E.B., K.G.W., S.C.C., J.S., O.N.K.-C., C.A., and J.P.G. designed research; C.E.B., K.G.W., D.A.-A., M.O., M.W., E.H., Z.M.T., J.P., E.G., F.Z., T.C., S.O., and J.P.G. performed research; C.E.B., S.C.C., and J.P.G. contributed unpublished reagents/analytic tools; C.E.B., K.G.W., D.A.-A., M.O., M.W., E.H., Z.M.T., J.P., F.Z., T.C., S.O., and J.P.G. analyzed data; C.E.B. and K.G.W. wrote the first draft of the paper; C.E.B., K.G.W., D.A.-A., Z.M.T., J.P., E.G., F.Z., T.C., S.O., J.S., O.N.K.-C., C.A., and J.P.G. edited the paper; C.E.B. and J.P.G. wrote the paper.

This work was supported by the National Institute of Neurological Disorders and Stroke (NINDS) Grant R01-NS-118037 and the National Institute of Aging Grant R01-AG-051902 (to J.P.G.). In addition, this work was supported by the NINDS P30 Core Grant P30-NS-045758 to the Center for Brain and Spinal Cord Repair. K.G.W. and S.M.O. were supported by the National Institute of Dental and Craniofacial Research Training Grant T32-DE-014320 and by the Ohio State University Presidential Fellowship. Z.M.T. was supported by the National Institute of Neurological Disorders Neuroimmunology Training Grant T32-NS-105864. T.C. was supported by the Thailand Research Fund-Royal Golden Jubilee Program (PHD/0146/2558; to T.C. and S.C.C.). We thank Julia Dziabis for her technical contributions to this work and Dr. Paolo Fadda at the Ohio State University Comprehensive Cancer Center Genomics Shared Resource (P30-CA-016058).

The authors declare no competing financial interests.

Correspondence should be addressed to Jonathan P. Godbout at jonathan.godbout@osumc.edu.

https://doi.org/10.1523/JNEUROSCI.1910-21.2022

Introduction

Traumatic brain injury (TBI) increases the prevalence of neuropsychiatric illness, with 15–30% of TBI patients experiencing cognitive decline, often comorbid with depression (Jackson et al., 2004; Himanen et al., 2006; Fleminger, 2008; Till et al., 2008; Silver et al., 2009; Wang et al., 2012). Furthermore, TBI correlates with increased risk of neurodegenerative diseases including chronic traumatic encephalopathy (CTE) and Alzheimer's disease (Bachstetter et al., 2015; Faul and Coronado, 2015; Lifshitz et al., 2016; Schaffert et al., 2018). In clinical studies of TBI, elevated metabolic activity, white matter abnormalities, and reactive microglia were detectable months after injury (Brooks et al., 2000; Ramlackhansingh et al., 2011; Johnson et al., 2013). Functional MRI analyses showed chronically activated microglia/macrophages in former NFL players with a history of concussions (Coughlin et al., 2015) and inflammation was detectable before cognitive impairment (Coughlin et al., 2017). PET studies revealed microglial activation in the thalamus that was associated with lower cognitive processing speed (Ramlackhansingh et al., 2011). Thus, it is plausible that chronic neuroinflammation and microglia dysfunction underlie these complications.

Microglia interpret signals from the periphery and may become primed after trauma (Norden et al., 2014). Following TBI, microglia priming is evident by increased gene expression of antigens (MHCII and CD11c), DAMPs, PAMPs (TLR2 and TLR4), scavenging and innate immunity (CD14, CD22, CD68; Norden et al., 2015). Primed microglia are hyper-responsive to immune challenges including lipopolysaccharide (LPS; Norden et al., 2015; Witcher et al., 2015). Indeed, primed microglia 30 d postinjury (dpi) were hyper-reactive to LPS challenge resulting in exaggerated microglial expression of IL1β, impaired cognition, and protracted sickness and depressive-like behaviors (Fenn et al., 2014; Muccigrosso et al., 2016). Collectively, TBI-induced microglial priming may contribute to chronic inflammation and functional decline.

Chronic microglial activation and neuropsychiatric dysfunction are detected in multiple models of TBI. For example, controlled cortical impact (CCI) elicited CD68$^+$ microglia detectable up to one year following injury (Loane et al., 2014). Repeated closed-head injury in mice increased Iba-1$^+$ (microglia) labeling that corresponded with deficits in hippocampal-dependent learning 12–18 months after injury (Mouzon et al., 2014). Furthermore, diffuse models of TBI lead to increased MHCII and CD68 expression, and altered microglia morphology in the cortex and hippocampus in mice (Fenn et al., 2014; Muccigrosso et al., 2016; Witcher et al., 2018). Recent single-cell RNA sequencing (scRNAseq) of the cortex 7 dpi showed unique clusters of trauma-associated microglia that were influenced by type 1 interferons (IFNs). This IFN pathway was robustly elevated during the subacute phase of injury (7 dpi) when there was a transition from acute to chronic inflammation with increased primed profiles of microglia (Witcher et al., 2021). Moreover, these TBI-associated microglia clusters were involved in dendritic remodeling, suppression of neuronal homeostasis, and cognitive impairment (Witcher et al., 2021). Administration of the CSF1R antagonist, PLX5622, is an established intervention to eliminate microglia (Elmore et al., 2015; McKim et al., 2018; Najafi et al., 2018; Witcher et al., 2018; Weber et al., 2019). As such, functional and cognitive deficits associated with diffuse TBI-induced chronic inflammation have been reversed by PLX5622-mediated elimination of microglia before TBI (Witcher et al., 2018, 2021). Thus, trauma-induced microglial priming represents an important target for intervention.

CSF1R antagonists have been used to force microglia turnover (Najafi et al., 2018; O'Neil et al., 2018), in which the remaining microglia self-renew following cessation of antagonism to repopulate the brain (Huang et al., 2018; Weber et al., 2019; Zhan et al., 2019). Forced microglial turnover in the chronic phase of CCI attenuated inflammation, reactive microglia (Nos2) and cognitive deterioration (Henry et al., 2020). Another CCI study involving microglia turnover showed regenerated microglia provided a reparative role in the hippocampus and were mediated by interleukin-6 (Willis et al., 2020). Therefore, the goal of this study was to force turnover of primed microglia that develop after diffuse TBI using CSF1R antagonism and determine whether this alleviated chronic inflammation, enhanced functional recovery, and attenuated immune reactivity.

Materials and Methods

Mice

Adult (six to eight weeks old) male C57BL/6 mice were purchased from Charles River Laboratories. Mice were housed in groups of four under a 12/12 h light/dark cycle with *ad libitum* access to food and water. Individual treatment groups were allotted based on body weight before surgery and injury procedures. All procedures were performed in accordance with the NIH *Guidelines for the Care and Use of Laboratory Animals* and were approved by The Ohio State University Institutional Animal Care and Use Committee.

Midline fluid percussion injury (mFPI)

Mice received a midline diffuse TBI using a FPI apparatus (Custom Design & Fabrication) as described previously (Fenn et al., 2014, 2015; Rowe et al., 2016; Witcher et al., 2018). Briefly, mice were anesthetized in an isoflurane chamber at 2–3% with a flow rate of 0.8 l/min. While anesthetized the surgical site was shaved and mice were maintained under anesthesia through fixation to a mouse stereotaxic (Stoelting Co, catalog #51731) with a gas anesthesia mask attachment (Stoelting Co, catalog #51609M). Once secured to the stereotaxic surgical sites were prepped with alternating swaps of iodine, 70% EtOH, and iodine once more. Mice then received a 3-mm craniectomy between the landmark sutures bregma and λ and a rigid Luer-loc needle hub was secured over the craniectomy site. Following this procedure, mice were moved to a heated (37°C) recovery cage and monitored until fully conscious (upright, responsive, walking). After recovery, mice were briefly re-anesthetized in an isoflurane chamber at 5% (flow rate 0.8 l/min) for 2 min, removed from the induction chamber, and the Luer-loc hub was filled with saline. The injury device was then attached to the hub and once a positive toe-pinch response was elicited (~30 s), a 10-ms pulse of saline (1.2 atm; 670–720 mV) was imposed on the dura (Kelley et al., 2007; Fenn et al., 2014; Lifshitz et al., 2016; Rowe et al., 2016). Immediately after injury, the hub was removed, dural integrity was confirmed, and mice were evaluated for injury severity using the self-righting test (Lifshitz et al., 2007; Witcher et al., 2018). Only mice with an intact dura and mild to moderate TBI were used (e.g., 200–540 s for self-righting time). In these studies, control mice were naive and uninjured. These naive controls (i.e., no craniectomy) were selected based on the 2 × 2 experimental design of the study and the endpoint of 30 dpi.

Postoperative/injury care

Mice with TBI were monitored for 1 h postinjury then allowed to recover overnight in a heated recovery cage with accessible food and hydrogel. The next day, mice were returned to their home cage. Based on our experimental design, no analgesics were provided in these studies. Mice were weighed and checked for signs of lethargy (lack of movement) and infection (redness and pus around the incision site) daily for the first 7 dpi and then once every other day for the duration of the experiments. Removal criteria included a loss of 20% of baseline bodyweight, sustained lethargy, paralysis, or surgical site infection. In the

current experiments, no TBI-injured mice met this exclusion criteria. Wound clips (7 mm) used to close the incision site were removed between 10 and 14 dpi.

Isolation of cells from bone marrow and spleen

Cells were isolated from bone marrow and spleen as described previously (McKim et al., 2016). Tissues were collected immediately following CO_2 asphyxiation. Spleens and femurs were collected in ice-cold PBS and mechanically disrupted through 70-µm nylon cell strainers. To collect bone marrow, the epiphyses of femurs were cut off and the marrow was flushed onto the 70-µm strainers with ice-cold PBS before disruption. Strainers were rinsed with PBS and samples were pelleted at $600 \times g$ for 6 min. Cell pellets were disrupted by vortex, washed with PBS, and the total number of cells was determined by the addition of counting beads (Thermo Fisher Scientific, catalog #01-1234-42) followed by flow cytometry.

Isolation of brain myeloid cells

$CD11b^+$ cells were isolated from whole brain homogenates as described previously (Wohleb et al., 2011, 2013, 2014) with minor modifications. In brief, brains were manually homogenized using Potter homogenizers and resulting homogenates were centrifuged at $600 \times g$ for 6 min. Supernatants were removed and cell pellets were resuspended in 70% isotonic Percoll (GE-Healthcare, catalog #45-001-747). A discontinuous isotonic Percoll density gradient was then layered as follows: 50%, 35%, and 0% (PBS). Samples were centrifuged for 20 min at $2000 \times g$, and cells were collected from the interphase between the 70% and 50% Percoll layers. These cells were referred to as enriched brain $CD11b^+$ cells based on previous studies demonstrating that viable cells isolated by Percoll density gradient yields >90% $CD11b^+$ cells (Wohleb et al., 2012).

Flow cytometry

Staining of cell surface antigens was performed as previously described (Wohleb et al., 2012; McKim et al., 2016). In brief, Fc receptors were blocked with anti-CD16/CD32 antibody (BD Biosciences, catalog #553144). Cells were washed and then incubated for 15 min at room temperature (RT) with the appropriate antibodies for: brain myeloid cells (CD45, BD Biosciences, catalog #550994 and CD11b, eBiosciences, catalog #17011283), bone marrow cells (Cd11b, Ter119, BD Biosciences, catalog #553673, B220, BD Biosciences, catalog #552772, Ly6C, BD Biosciences, catalog #560525, Ly6G, BD Biosciences, catalog #5511460) and spleen cells (Ter119, B220, CD3, Ly6C, Cd11b, Ly6G, BD Biosciences, catalog #557596). Cells were washed and resuspended in PBS for analysis. Antigen expression was determined using a modified Becton-Dickinson FACSCalibur ninne-color three laser cytometer (BD Biosciences). Data were analyzed using FlowJo software (version 10.1; BD Biosciences) and positive labeling for each antibody was determined based on isotype-stained controls. Nonspecific binding was assessed using isotype-matched antibodies.

PLX5622-mediated elimination and repopulation of microglia

A paradigm of forced microglial turnover was used (O'Neil et al., 2018; Henry et al., 2020) with modifications. In brief, CSF1R antagonist PLX5622 (Plexxikon) was formulated in AIN-76A rodent chow by Research Diets Inc. at a concentration of 1200 ppm or ~1200 mg/kg. Standard AIN-76A diet was provided as control. At 7 dpi, mice received *ad libitum* access to PLX5622 or vehicle diet for 7 d. This dosage depleted over 95% of microglia in C57BL/6 mice (McKim et al., 2018; Weber et al., 2019; Witcher et al., 2021). After 7 d of depletion, PLX5622 containing diets were removed and mice were returned to standard rodent chow for the duration of the experiment. Mice were afforded over two weeks for the repopulation of PLX5622-sensitive cells (microglia and tissue macrophages).

RNA extraction and NanoString gene expression analysis

At 30 dpi, cortical samples were dissected, flash-frozen, homogenized and RNA was extracted (Tri-Reagent, Sigma). RNA integrity was confirmed by Agilent BioAnalyzer and preamplification cycles were determined using expression of housekeeping genes (*Gapdh*). Gene expression was quantified using the NanoString neuropathology panel with 30 added genes (760 genes; Witcher et al., 2021). Technical normalization was performed to positive and negative controls and data were validated using housekeeping genes (*Aars*, *Ccdc127*, *Csnk2a2*, *Fam104a*, *Lars*, *Mto1*) based on strong correlation with total counts ($R^2 > 0.8$). Data were normalized and differential expression testing was performed using DESeq2 in R (Love et al., 2014). In brief, EstimateSizeFactors in DESeq2 was used for normalization to housekeeping genes. The DESeq design parameter included two variables: one controlling for NanoString cartridge and a second for experimental group (four levels: CON-Veh, CON-Repop, TBI-Veh, TBI-Repop). Results tables were generated for pairwise comparisons of interest (i.e., TBI-Veh vs CON-Veh; TBI-Repop vs TBI-Veh). Genes were considered significant if $p < 0.05$. Heatmap was generated using pheatmap in R with scale = "row," which centers and scales values by gene such that colors reflect Z-scores rather than absolute values. Statistically significant genes were subsequently used for Ingenuity Pathway Analysis (IPA; QIAGEN). Gene names and fold changes were submitted to compare expression patterns in our dataset to IPA's database. IPA results for canonical pathways ($p < 0.05$; composite z score > 2) were considered significant. Upstream regulators were further filtered for activation z scores (positive or negative) that were associated with either increased or decreased signaling.

Iba-1 and MBP immunofluorescence

Mice were transcardially perfused with PBS followed by 4% paraformaldehyde (PFA). Brains were removed, postfixed, and dehydrated in 30% sucrose. Cortical sections (30 µm) were collected, blocked (0.1% Triton X-100, 5% BSA, and 5% NDS) and incubated with primary antibodies for either anti-Iba1 (rabbit anti-Iba1, 1:1000, Wako catalog #019-19471, RRID:AB_2665520) or anti-MBP (rabbit anti-MBP, 1:500, ThermoFisher catalog #Mm01266402_m1). Next, sections were washed and incubated with a fluorochrome-conjugated secondary antibody (donkey anti-rabbit; Alexa Fluor 488/594/647; Invitrogen catalog #A-21 206/R37119/A-31573). Fluorescent labeling was visualized and imaged using an EVOS FL Auto 2 imaging system (Thermo Fisher Scientific). To determine percent area of $Iba1^+$ labeling, single-channel images were converted to eight-bit TIFF format and constant thresholds were used to quantify positively labeled pixels (ImageJ software). To determine the percent of MBP^+ myelinated cortex (van Tilborg et al., 2017) the area of Mbp^+ labeling in the cortex was traced and divided from the total area of the image × 100. Values from four to six images per mouse were averaged and used to calculate group averages and variance for each injury or treatment group. IHC data were analyzed by an investigator blinded to treatment groups.

Compound action potential (CAP) recording

CAPs in the corpus callosum were recorded in *ex vivo* slice preparations as described previously (Witcher et al., 2021). In brief, coronal brain sections (400 µm) were collected and transferred to chambers containing artificial CSF (aCSF), allowed to incubate at 37°C for 30 min, then RT for 1 h. A gravity perfusion system was used for solution exchange (2–3 ml/min) with oxygenated aCSF in a submerged chamber at RT. Borosilicate glass electrodes filled with aCSF (1.5–3 MΩ) were positioned ~1.5 mm apart to record electrically stimulated CAPs. Stimulation intensities (0–2 mA, 21 steps, 200 µS, every 5 s) were applied to create intensity-response plots. Data were digitized using an Axopatch 200B amplifier, Digidata 1440A, and pClamp 10.6 software (Molecular Devices), and Clampfit 10.6 software. Peak values from three sections per mouse were averaged to generate N1 and N2 values used to calculate group means and error. Area under the curve (AUC) was calculated to synthesize evoked stimulus recordings into a single metric. CAP recording data were analyzed by an investigator blinded to treatment groups.

DiI staining and dendritic spine analysis

To assess neuronal plasticity, cortical dendritic spine density and morphology were determined as described previously (Erion et al., 2014; Hao et al., 2016). In brief, coronal brain sections (1 mm) were collected

using a rodent brain matrix and fixed in 4% PFA for 1 h. Sections were washed and 1′dioctadecyl-3,3,3′3-tetramethlindocarbocyanine perchlorate (DiI) crystals were applied for 48–72 h at RT then were washed, mounted, and coverslipped. For analysis, a series of z-stacks were taken from cortical Layer IV/V using a Leica SP8 confocal microscope (Leica Biosystems). Neuronal morphology was assessed with Imaris software 7.0 (Bitplane, Oxford Instrument Company). Dendritic spine counts were calculated from 3D construction using semi-automatic filament tracing.

Cognitive and depressive-like behavior

To assess cognitive function following TBI, novel object location (NOL) and novel object recognition (NOR) were determined as previously described (Witcher et al., 2021). These tests involved four 10-min phases each separated by 24 h: habituation (no objects), acclimation (two objects), location (two objects, one new location), and recognition (two objects, with one new object). Discrimination index in the location and recognition trials was determined $[(time_{novel} - time_{familiar})/time_{total}] \times 100$ (Denninger et al., 2018). To measure depressive-like behavior 30 dpi, tail suspension test (TST) was performed as described previously (Corona et al., 2013; Fenn et al., 2014). In brief, mice were suspended by their tail in a $32 \times 33 \times 33$ cm box and the duration of immobility was determined over a 5-min period. Trials for each behavior were videotaped and analyzed by an investigator blinded to treatment groups.

LPS challenge and behavior

Mice were injected (intraperitoneally) 30 dpi with saline or LPS (0.5 mg/kg; serotype 0127:B8; Sigma-Aldrich). Unmotivated locomotor and motivated social interaction were assessed 24 h following saline or LPS injection to evaluate sickness behavior. Activity was measured in separate, 5 min trials in an open field apparatus ($40 \times 40 \times 25$ cm; Omnitech Electronics), in which a novel juvenile mouse was added to the apparatus for the social exploration trial. All video trials of locomotive behavior (moving around the cage, grooming) and social interaction (anogenital sniffing, trailing) were analyzed by an investigator blinded to treatment groups.

RNA extraction and qPCR

A coronal brain section (1 mm) was collected using a brain matrix and RNA was extracted using the TriReagent protocol (Sigma-Aldrich), normalized by concentration, and reverse-transcribed to cDNA. The Applied Biosystems Taqman Gene Expression assay-on-demand protocol and recommended probes for each gene of interest was used for quantitative real-time PCR. Target gene (*Ccl2*, Mm00441242_m1; *Il1β*, Mm00434228_m1; *Tlr4*, Mm00445273_m1) and reference gene (*Gapdh*, Mm99999915_g1) expression was determined using a QuantStudio 5 (Thermo Fisher Scientific) and data were analyzed using the comparative threshold method (ΔΔCt) with data expressed as fold change from control.

Statistical analysis

GraphPad Prism software was used for ANOVA of histologic, behavioral, and electrophysiological data. One-way, two-way, three-way or repeated-measures ANOVA was used to determine main effects and interactions between factors. Bonferroni's test for multiple comparisons was used for *post hoc* analysis when main effects and/or interactions were determined. a priori comparisons were determined by Student's *t* test; $p < 0.05$ was considered significant.

Results

PLX5622-mediated elimination and repopulation of myeloid cells

The goal of this study was to force turnover of "trauma-associated" or primed microglia that develop after diffuse TBI (Witcher et al., 2018, 2021) and determine whether this alleviated chronic inflammation, enhanced functional recovery and attenuated immune reactivity 30 dpi. This forced turnover experimental design (Fig. 1*D*) is similar to approaches published previously in murine models of aging (O'Neil et al., 2018; Najafi et al., 2018) and psychological stress (Weber et al., 2019). As originally described (Elmore et al., 2014, 2015), this CSF1R antagonist causes significant elimination of microglia of C57BL/6 mice by 7 d (McKim et al., 2018; Witcher et al., 2018, 2020). Moreover, cessation of PLX5622 leads to the self-renewal of microglia within days (Huang et al., 2018; Zhan et al., 2019) and these microglia fully repopulate within 21 d (Elmore et al., 2015; Najafi et al., 2018; Weber et al., 2019). Hence, this process of elimination and repopulation of microglia is termed forced turnover.

For initial controls, we first confirmed that oral administration of PLX566 (1200 ppm) significantly reduced the number of microglia based on cell surface expression of CD11b and CD45. Figure 1*B*,*C* shows that the 7-d administration of PLX5622 resulted in over 97% reduction in the percentage of $CD11b^+/CD45^{lo}$ microglia in the brain ($p < 0.0001$). Next, we forced microglial turnover after TBI, starting at 7 dpi and ending 30 dpi (Fig. 1*D*). Iba-1 histology was used to assess elimination at 14 dpi (7 d of PLX) and repopulation at 30 dpi (16 d after PLX cessation). Figure 1*E*,*F* shows that this PLX5622 protocol was efficient in the elimination of microglia based on the robust reduction in Iba-1 expression in the cortex ($Iba\text{-}1^+$ % area). These data parallel the cell surface expression of CD11b and CD45 shown in Figure 1*B*,*C*. In addition, Figure 1*E*,*G* shows subsequent repopulation of microglia in the cortex by 30 dpi ($Iba\text{-}1^+$ % area). Notably, the TBI-Veh group had the highest percentage of $Iba\text{-}1^+$ area in the cortex 30 dpi, compared with all other groups ($p < 0.05$).

It is important to note that PLX5622 can affect a percentage of peripheral myeloid cells, mostly $CSF1R^+$ tissue macrophages (Lee et al., 2018; Lei et al., 2020). Thus, we assessed the percentage of immune cells in the bone marrow and spleen with this forced turnover protocol at the 30d end point. TBI groups were not included in this experiment. For the bone marrow analyses (Fig. 1*H*,*I*), there were no difference the cell percentages of monocytes ($Ter119^-$, $Cd11b^+$, $Ly6C^+$, $Ly6G^-$), granulocytes ($Ter119^-$, $Cd11b^+$, $Ly6C^+$, $Ly6G^+$), B-cells ($Ter119^-$, $Cd11b^-$, $B220^+$), or other lymphocytes ($Ter119^-$, $Cd11b^-$, $B220^-$) between vehicle and PLX-Repop groups. The same results were apparent in the spleen (Fig. 1*J*,*K*). There were no differences in the cell percentages of monocytes ($Ter119^-$, $Cd11b^+$, $Ly6C^+$, $Ly6G^-$), granulocytes ($Ter119^-$, $Cd11b^+$, $Ly6C^+$, $Ly6G^+$), B-cells ($Ter119^-$, $Cd11b^-$, $B220^+$), or T-cells ($Ter119^-$, $Cd11b^-$, $CD3^+$) between vehicle and PLX-Repop groups. While it is possible that myeloid cells in the periphery were affected by PLX elimination, they were at baseline numbers with the cessation of PLX at 30 d. Last, it is important to note that peripheral myeloid cells, such as monocytes, are turned over naturally by the immune system (e.g., bone marrow or self-renewal) at a significantly higher rate compared with microglia.

Forced microglial turnover attenuated persistent neuropathology-related mRNA expression in the cortex 30 dpi

We recently reported that microglia depletion before TBI ablated cortical inflammation (Witcher et al., 2021). The subacute phase of inflammation (7 dpi) was characterized by increased IFN responses and evidence of microglial priming (Witcher et al., 2021). Thus, we aimed to use a forced microglia turnover design to target the "primed" or "trauma associated" microglia that develop following diffuse TBI. Moreover, we aimed to determine whether this forced turnover after TBI prevented chronic

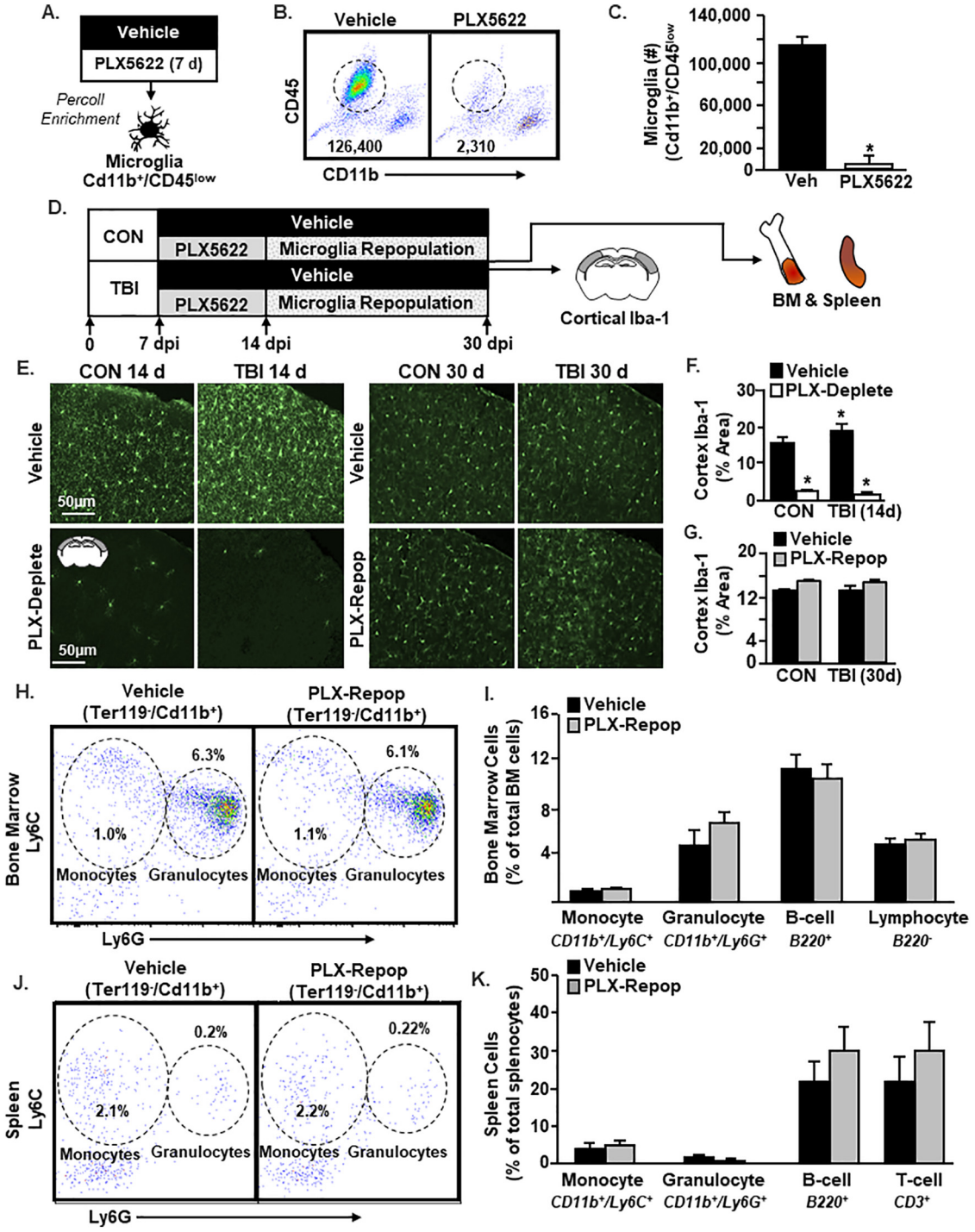

Figure 1. PLX5622-mediated elimination and repopulation of brain myeloid cells. ***A***, Adult male C57BL/6 mice were provided diets formulated with either vehicle or a CSF1R antagonist (PLX5622; PLX) at for 7d. Brain myeloid cells were enriched by Percoll isolation, and the percentage of microglia were determined in the brain ($n = 3$). ***B***, Representative bivariate dot plots of CD11b/CD45 labeling of Percoll-enriched cells. ***C***, Number of microglia ($CD11b^+/CD45^{low}$) in the brain, normalized to control counting beads. ***D***, Adult male C57BL/6 mice were subjected to mFPI (TBI) or left as uninjured controls (CON). At 7 dpi, mice were provided diets formulated with either vehicle or a CSF1R antagonist (PLX5622; PLX) for 7 d and then returned to standard chow 14 dpi. At 30 dpi (16 d of microglia repopulation), microglial histology ($Iba\text{-}1^+$ labeling) was determined. ***E***, Representative images of $Iba\text{-}1^+$ labeling in the cortex 14 dpi (PLX-Depletion) and 30 dpi (PLX-Repop). Percent area of $Iba\text{-}1^+$ microglia (***F***) 14 dpi and (***G***) 30 dpi ($n = 6$). In a parallel experiment using this design, the percentage of cells in the bone marrow and spleen were determined at the 30-d endpoint (16 d of repopulation). ***H***, Representative bivariate dot plots of Ly6C/Ly6G labeling of $Terr119^-/Cd11b^+$ cells isolated from the bone marrow after 16 d of repopulation. ***I***, Percentage of monocytes, granulocytes, B-cells, and other lymphocytes in the bone marrow after 14 d of repopulation ($n = 6$). ***J***, Representative bivariate dot plots of Ly6C/Ly6G labeling of $Ter119^-/Cd11b^+$ cells isolated from the spleen after 16 d of repopulation. ***K***, Percentage of monocytes, granulocytes, B-cells, and T-cells in the spleen after 16 d of repopulation ($n = 6$). Bars represent the mean ± SEM. Means with * are significantly different from control ($p < 0.05$).

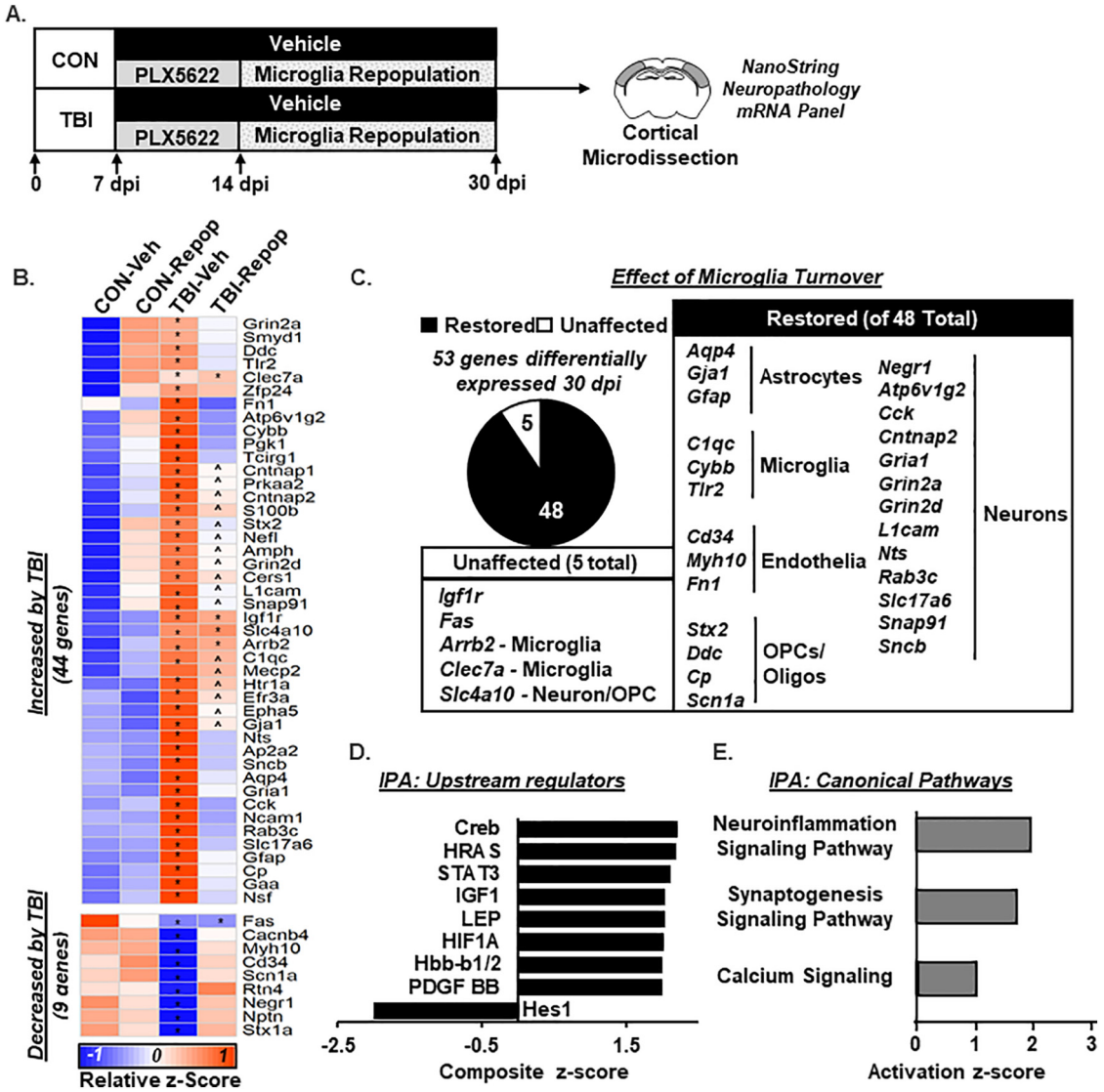

Figure 2. Forced microglial turnover attenuated persistent neuropathology-related mRNA expression in the cortex 30 dpi. ***A***, Adult male C57BL/6 mice were subjected to mFPI (TBI) or left as uninjured controls (CON). At 7 dpi, mice were provided diets formulated with either vehicle or a CSF1R antagonist (PLX5622; PLX) for 7d and then returned to standard chow 14 dpi. At 30 dpi (16 d of microglia repopulation), cortical mRNA expression (NanoString neuropathology panel) in the cortex was determined ($n = 6$). ***B***, Heatmap shows the relative *z* score of mRNA that was differentially expressed by TB1 and influenced by PLX-Repop. Means with * are significantly different from CON-Veh ($p < 0.05$) and means with [a] are significantly different from both CON-Veh and TB1-Veh ($p < 0.05$). ***C***, Pie chart represents genes unaffected (5 genes) or restored (48 genes) following microglial turnover after TBI. Select genes are shown and annotated if the gene is predominately expressed by a primary cell-type (Brain RNAseq, www.brainrnaseq.org). IPA of (***D***) significant upstream regulators (composite *z* score, $p < 0.05$) and (***E***) significant canonical pathways (activation *z* score, $p < 0.05$) of the differentially expressed genes based on their respective *z* score are shown.

microglia-mediated inflammation and improved functional recovery.

To address these objectives, we forced microglial turnover after TBI starting at 7 dpi and ending 14 dpi, with repopulation until 30 dpi (Fig. 2*A*). Cortical neuropathology was assessed 30 dpi using a NanoString neuropathology panel (Fig. 2*B–E*). There were 53 genes related to neuropathology and inflammation that were differentially expressed in the cortex 30 dpi ($p_{adj} < 0.05$). Of these, 44 genes were increased, and 9 genes were decreased in the cortex 30 dpi (relative *z* score, $p_{adj} < 0.05$; Fig. 2*B*). TBI-induced increases in pro-inflammatory genes including *C1qc*, *Tlr2*, *Mecp2*, *Cybb*, and S100β were reversed by forced microglial turnover ($p_{adj} < 0.05$; Fig. 2*B*). Several astrocytic associated genes, including *Aqp4* and *Gfap* and were increased 30 dpi and restored by microglial turnover ($p_{adj} < 0.05$; Fig. 2*B*). Furthermore, genes associated with excitatory glutamatergic transmission (*Gria1*, *Gria2a*, *Gria2d*, *Slc17a6*), neurodegenerative conditions including dementia (*Sncb*), epilepsy (*Cntnap2*, *Scn1a*), and serotonin deficiency associated with psychological disorders (*Ddc*) were increased 30 dpi and reversed with microglial turnover ($p_{adj} < 0.05$; Fig. 2*B*).

Next, each differentially expressed gene was examined using the Barres laboratory's Brain RNAseq search engine (www.brainrnaseq.org). This search engine provided additional information to which CNS cell primarily expressed the genes of interest. Figure 2*C* shows that 48 genes induced by TBI were reversed by forced turnover and five genes (*Igfr1*, *Fas*, *Arrb2*, *Clec7a*, *Slca10*) were unaffected by turnover. The 48 differentially expressed genes after TBI were associated with microglia, astrocytes, neurons, and endothelia. Moreover, the majority of genes increased 30 dpi and reversed by forced turnover were associated with neurons (*Gria1*, *Gria2a*, *Gria2d*, *Slc17a6*, *Nts*, *Negr1*, *Sncb*, *Cck*). Overall, the turnover of microglia after TBI influenced the mRNA profile of several cell types including microglia, astrocytes, and neurons.

IPA of upstream regulators ($p < 0.05$; composite z score > 2) indicated gene expression patterns post-TBI consistent with cytokine and IFN signaling (*Stat3*), growth factors (*Igf*, *Pdgf*), homeostasis (*Hif1a*, *Lep*), metabolism (*Hbb-b1/2*), and cAMP signaling (CREB; Fig. 2*D*). Canonical pathways ($p < 0.05$; activation z score > 2) associated with neuroinflammation, synaptogenesis and calcium signaling were increased in the cortex 30 dpi (Fig. 2*E*). Collectively, the neuropathological mRNA profile in the cortex 30 dpi was reversed by the forced turnover of microglia.

Forced turnover of microglia attenuated deficits in neuronal connectivity 30 dpi

Our previous transcriptome profiling studies indicated that microglia mediate chronic inflammation (30 dpi) and neuronal pathology after diffuse TBI (Witcher et al., 2018, 2021). Furthermore, increased dendritic remodeling in the cortex 7 dpi and impaired neuronal connectivity 30 dpi were blocked by microglial ablation (PLX5622 mediated) before TBI (Witcher et al., 2021). Here, the influence of TBI and forced microglial turnover on dendritic complexity (dendritic volume, area, and spine density), neuronal connectivity, and myelin basic protein (MBP) content were assessed 30 dpi (Fig. 3*A*). Figure 3*B* shows representative DiI^+ labeling of cortical dendrites. Spine volume ($F_{(1,52)} = 5.2$, $p < 0.04$; Fig. 3*C*) and spine area ($F_{(1,52)} = 6.5$, $p < 0.02$; Fig. 3*D*) were increased by TBI 30 dpi. These increases in spine volume and area, however, were unaffected by microglial turnover. Dendritic spine density was also unaffected by TBI and microglia turnover 30 dpi (Fig. 3*E*). Thus, the persistent alterations in dendritic morphology 30 dpi in the cortex were not influenced by the forced turnover of microglia.

Because diffuse TBI impacts axons that project throughout the cortical layers and into the corpus callosum (Ramos et al., 2008), we examined whether microglial turnover restored neuronal connectivity 30 dpi. Here, CAPs were stimulated and recorded from the corpus callosum of *ex vivo* brain slices (Fig. 3*A*). Representative tracings show distinct N1 and N2 changes of the action potential between CON-Veh and TBI-Veh mice 30 dpi (Fig. 3*F*). N1 represents fast-conducting fibers (large, myelinated) and N2 represents slow-conducting fibers (small, unmyelinated). The N1 and N2 components of the action potential are shown at 30 dpi (Fig. 3*G–K*).

Figure 3*G* shows that the N1 component of CAP was influenced by TBI ($F_{(1,16)} = 4.4$, $p < 0.03$), Repopulation ($F_{(1,16)} = 83.3$, $p < 0.001$), and an interaction between TBI × Repopulation ($F_{(1,16)} = 2.9$, $p < 0.04$). These interactions were evident in the AUC analysis of the N1 amplitude (Fig. 3*I*). *Post hoc* analysis shows that the N1 amplitude in the AUC was increased in the CON-Repop group compared with the CON-Veh group ($p < 0.0001$; Fig. 2*I*). Moreover, the N1 amplitude in the AUC was reduced in the TBI-Veh group compared with all other groups ($p < 0.03$) including the TBI-Repop group ($p < 0.001$; Fig. 3*I*). Thus, the N1 amplitude was reduced by TBI 30 dpi and increased by the repopulation of microglia.

Figure 3*H* shows that the N2 component of CAP was influenced by TBI ($F_{(1,16)} = 5.2$, $p < 0.04$). These differences were evident in the AUC analysis of the N2 amplitude (Fig. 3*J*). *Post hoc* analyses confirmed that the N2 amplitude was decreased in TBI-Veh mice compared with all other treatment groups ($p < 0.0004$) including the CON-Veh group ($p < 0.003$; Fig. 3*J*). The N2 values were not different between the CON-Veh, CON-Repop, and TBI-Repop treatment groups. Collectively, there were reductions in CAPs in both the N1 and N2 fibers 30 dpi that were no longer detected after the forced turnover of microglia.

Alterations in myelin and corresponding white matter damage are other issues related to brain injury that may adversely affect neuronal plasticity and connectivity (Marion et al., 2018). To assess potential differences in white matter, MBP labeling was determined in the cortex 30 dpi (van Tilborg et al., 2017). The proportion of MBP^+ labeling in the cortex was increased 30 dpi ($F_{(1,23)} = 5.840$, $p < 0.03$; Fig. 2*K*,*L*). While there was a main effect of TBI on increased MBP^+ labeling in the cortex, this was unaffected by microglia turnover. Overall, forced turnover of microglia improved TBI-associated deficits in neuroconnectivity (N1 and N2 components of action potential) that were independent of dendritic remodeling or MBP content in the cortex.

Cognitive deficits and depressive-like behavior 30 dpi were ameliorated by microglial turnover

Depressive-like behavior and cognitive decline are two impairments that influence functional recovery after TBI. For instance, cognitive dysfunction after diffuse TBI in mice was evident in the Barnes maze, NOL, and NOR tasks 30 dpi (Muccigrosso et al., 2016; Witcher et al., 2021). Thus, we sought to determine whether microglial turnover improved behavioral and cognitive recovery 30 dpi (Fig. 4*A*). Mice were injured or left as controls and were subjected to the turnover protocol at 7 dpi.

In the first experiment, depressive-like behavior was assessed by the TST 30 dpi (Fig. 4*B*). There was a main effect of TBI on time spent immobile ($F_{(1,40)} = 15.7$, $p < 0.0004$). This TBI-associated immobility was dependent on microglial turnover (interaction, $F_{(1,40)} = 5.9$, $p < 0.03$). *Post hoc* analysis confirmed that the TBI-Veh group spent the most time immobile ($p < 0.05$; Fig. 4*B*). Time spent immobile was not different between the CON-Veh, CON-Repop, and TBI-Repop treatment groups. Collectively, depressive-like behavior 30 dpi was attenuated by the forced turnover of microglia.

In a second experiment, cortical and hippocampal function were assessed using the NOL and NOR memory tasks (Antunes and Biala, 2012; Denninger et al., 2018; Witcher et al., 2021). In the same mice, NOL was assessed 30 dpi and then NOR was assessed 1 d later (i.e., 31 dpi). The first phase of the test examined location and the second phase examined recognition recall. There were no significant differences in total time spent exploring the objects between the four experimental groups during either task (Fig. 4*C*, *F*). NOL was influenced by TBI and forced microglial turnover (interaction, $F_{(1,44)} = 12.69$, $p < 0.001$). *Post hoc* analysis confirmed that TBI-Veh mice investigated the object in the novel location for less time compared with all other groups, including the TBI-PLX-Repop mice ($p < 0.0003$; Fig. 4*D*). These interactions were also evident in the discrimination index for NOL, as TBI-Veh mice spent more time with the object in the familiar location compared with all other groups ($p < 0.0003$; Fig. 4*E*).

Similar to NOL, there was also an interaction between TBI and forced microglial turnover for recognition of a novel object (interaction, $F_{(1,37)} = 24.37$, $p < 0.0001$). *Post hoc* analysis confirmed that TBI-Veh mice investigated the novel object for less time compared with all other groups ($p < 0.0001$; Fig. 4*G*). TBI-Veh mice also had a diminished discrimination index for the novel object compared with all other groups ($p < 0.0001$; Fig. 4*H*). TBI-PLX-Repop mice did not have reductions in either time spent investigating the novel object or discrimination index. Collectively, the cognitive impairment in NOL/NOR evident 30 dpi was attenuated by forced microglial turnover.

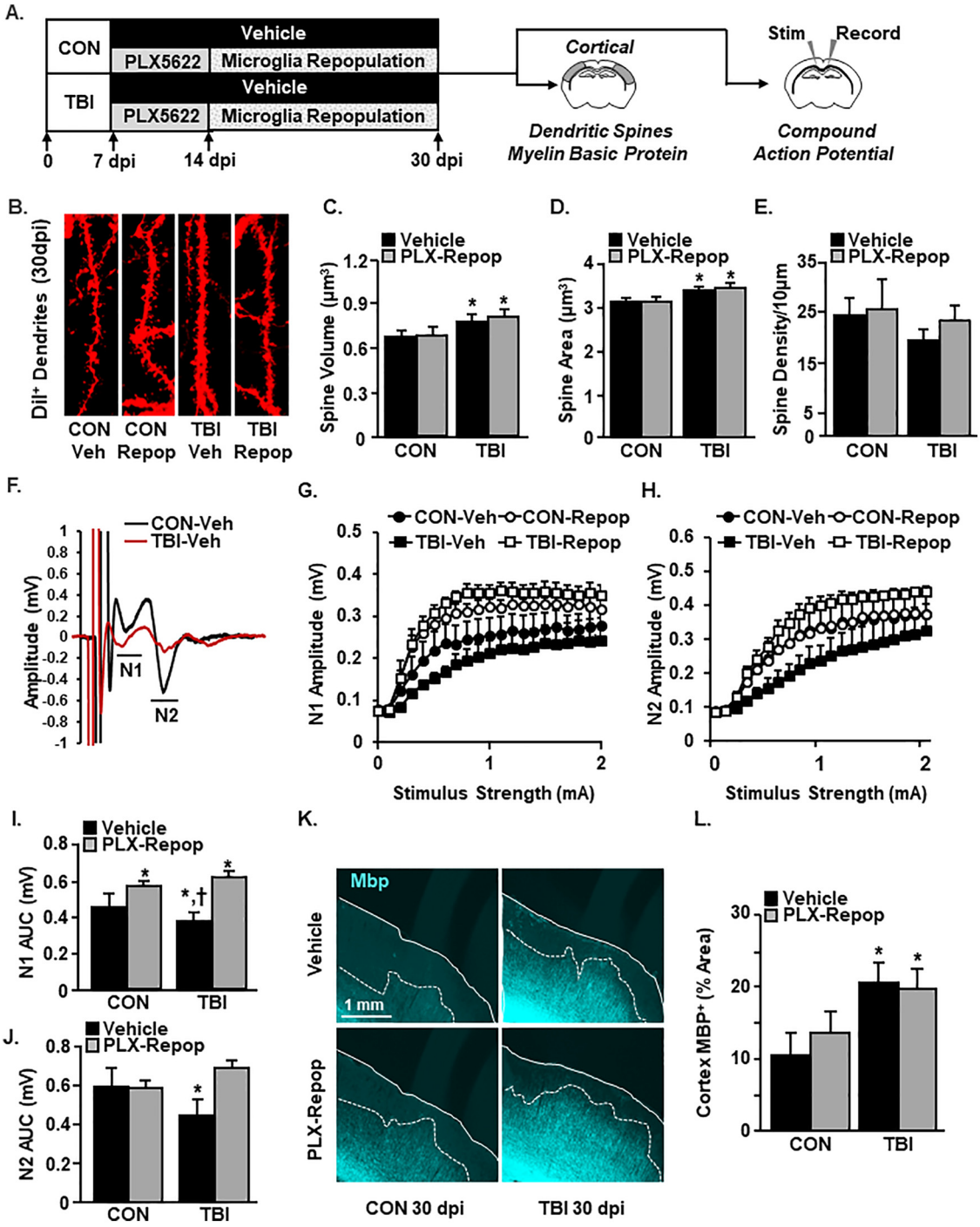

Figure 3. Forced turnover of microglia attenuated deficits in neuronal connectivity 30 dpi. ***A***, Adult male C57BL/6 mice were subjected to mFPI (TBI) or left as uninjured controls (CON). At 7 dpi, mice were provided diets formulated with either vehicle or a CSF1R antagonist (PLX5622) for 7 d and then returned to their standard rodent chow at 14 dpi. At 30 dpi (16 d of microglia repopulation), mice were killed, and tissues were collected for analysis of dendritic spines, MBP, or CAPs. ***B***, Representative cortical images of Dil^+ dendrites 30 dpi from each treatment group are shown ($n = 6$). Bar graphs represent (***C***) dendritic spine volume, (***D***) dendritic spine area, and (***E***) dendritic spine density. ***F***, CAPs were stimulated and measured from *ex vivo* preparation of the corpus callosum ($n = 4$) and representative N1 and N2 tracings of CAP from control and TB1 mice 30 dpi are shown. Graphs represent average recording amplitude across a range of stimulus intensities for (***G***) N1 and (***H***) N2. AUC determined for the (***I***) N1 and ***J***) N2 amplitudes. ***K***, Representative cortical images of MBP^+ labeling 30 dpi from each treatment group ($n = 6$). ***L***, Percent MBP^+ labeling in cortical sections. Graphs represent mean ± SEM. Means with * are significantly different from CON-Veh ($p < 0.05$) and means with † are significantly different from both CON-Veh and PLX-Repop ($p < 0.05$).

Immune reactivity 30 dpi was reduced by forced turnover of microglia

One functional consequence of microglia priming after TBI is immune reactivity to peripheral immune challenge. For example, we previously reported that immune challenge with LPS 30 dpi caused an exaggerated inflammatory cytokine response in the brain, associated with prolonged sickness behavior and cognitive impairment (Fenn et al., 2014; Muccigrosso et al., 2016). Thus, we examined whether forced turnover of microglia attenuated the increased immune reactivity of TBI mice to LPS challenge. Mice were injured or left as controls and were subjected to the turnover protocol at 7 dpi. At 30 dpi, mice were injected

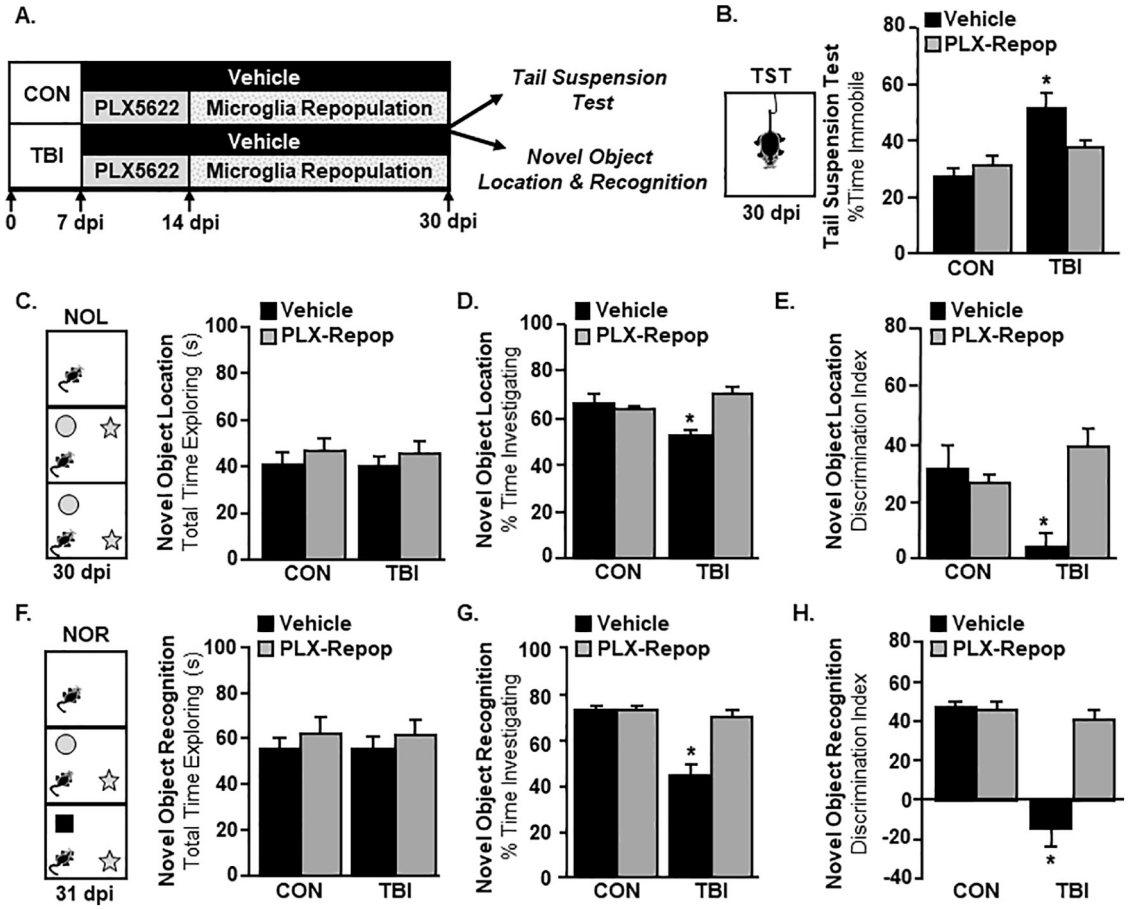

Figure 4. Cognitive deficits and depressive-like behavior 30 dpi were ameliorated by microglial turnover. ***A***, Adult male C57BL/6 mice were subjected to mFPI (TBI) or left as uninjured controls. At 7 dpi, mice were provided diets formulated with either vehicle or a CSF1R antagonist (PLX5622) for 7 d, and then returned to standard rodent chow at 14 dpi. At 30–31 dpi (16 d of microglia repopulation), depressive-like behavior ($n = 9$) and cognition ($n = 12$) were assessed. ***B***, Percentage of time immobile in the TST at 30 dpi. In a separate cohort, mice were used in the NOL and NOR tests. For NOL at 30 dpi, (***C***) time spent exploring the arena, (***D***) percentage of time spent investigating the object location, and (***E***) discrimination index for the object location were determined. For NOR at 31 dpi, (***F***) time spent exploring the arena, (***G***) percent of time spent investigating the novel object, and (***H***) discrimination index for the novel object were determined. Graphs represent mean ± SEM. Means with * are significantly different from CON-Veh ($p < 0.05$).

intraperitoneally with saline or LPS and several behavioral and biochemical parameters were assessed (Fig. 5*A*).

In the assessment of lethargy, locomotor activity was reduced by LPS at each time point ($F_{(1,63)} = 77.8$, $p < 0.0001$; Fig. 5*B*). There was no effect of the repopulation of microglia in the control, uninjured groups, on locomotor activity. For instance, the control mice (CON-Veh-Saline, CON-Repop-Saline) had the same baseline locomotion during the testing that was independent of microglial turnover. *Post hoc* analyses indicate TBI-Veh-LPS mice had reduced locomotor activity compared with all groups at 12 h ($p < 0.05$) and 24 h post-LPS ($p < 0.0001$; Fig. 4*B*, *C*). Both TBI-Repop-LPS and CON-Veh-LPS groups returned to baseline activity by 12 h after LPS, so only the TBI-Veh-LPS mice had extended lethargy after LPS injection.

In the motivation to engage in social behavior with a juvenile (i.e., social exploratory behavior), there was an LPS-dependent reduction at 4 h ($F_{(1,63)} = 29.6$, $p < 0.001$), 8 h ($F_{(1,63)} = 24.0$, $p < 0.001$), and 12 h ($F_{(1,62)} = 9.13$, $p < 0.004$; Fig. 5*D*). Again, there was no effect of the repopulation of microglia in the control, uninjured groups, on social exploratory behavior. For example, the control mice (CON-Veh-Saline and CON-Repop-Saline) had the same baseline social interaction during the testing that was independent of turnover. *Post hoc* analysis confirmed that TBI-Veh-LPS mice had reduced social exploratory behavior compared with all other groups 24 h post-LPS ($p < 0.02$; Fig. 5*E*). TBI-PLX-Repop mice returned to baseline social exploratory behavior by 24 h and were at the same levels as CON-Veh-LPS mice. Taken together, only the TBI-Veh-LPS mice had prolonged lethargy and social withdrawal after LPS challenge, these behavioral deficits were not present in control mice or TBI mice that had the intervention of forced microglial turnover.

One functional aspect of microglial reactivity is prolonged expression of cytokines and chemokines in the brain after LPS challenge (Norden et al., 2015). The resolution of the neuroinflammatory response to LPS (0.5 mg/kg, i.p.) in adult heathy C57BL/6 mice is between 24–72 h (Wynne et al., 2009; Witcher et al., 2015; O'Neil et al., 2018). The cortex is a brain region in which long-term alterations in glial profiles were detected after diffuse TBI caused by mFPI (Fenn et al., 2014; Witcher et al., 2021). Thus, mRNA expression of several inflammatory related genes, *Ccl2*, *Il1b*, *Tlr4*, was determined from coronal brain sections collected through the cortex at 24 and 72 h post-LPS (Fig. 5*F*) At 24 h after LPS, was an LPS-dependent increase in mRNA levels of *Ccl2, Il1b*, and *Tlr4* ($F_{(1,39)} = 16.7$, $p < 0.001$, for each). At 24 h, however, these genes were not influenced by either TBI or forced turnover.

Figure 4*F* also shows that there was still an effect of LPS at 72 h on mRNA levels of *Ccl2*, *Il1b*, and *Tlr4* ($F_{(1,64)} = 14.3$, $p < 0.001$, for each). For *Il1b*, only the TBI-Veh-LPS group was significantly different ($p < 0.05$) from controls (Con-Veh-

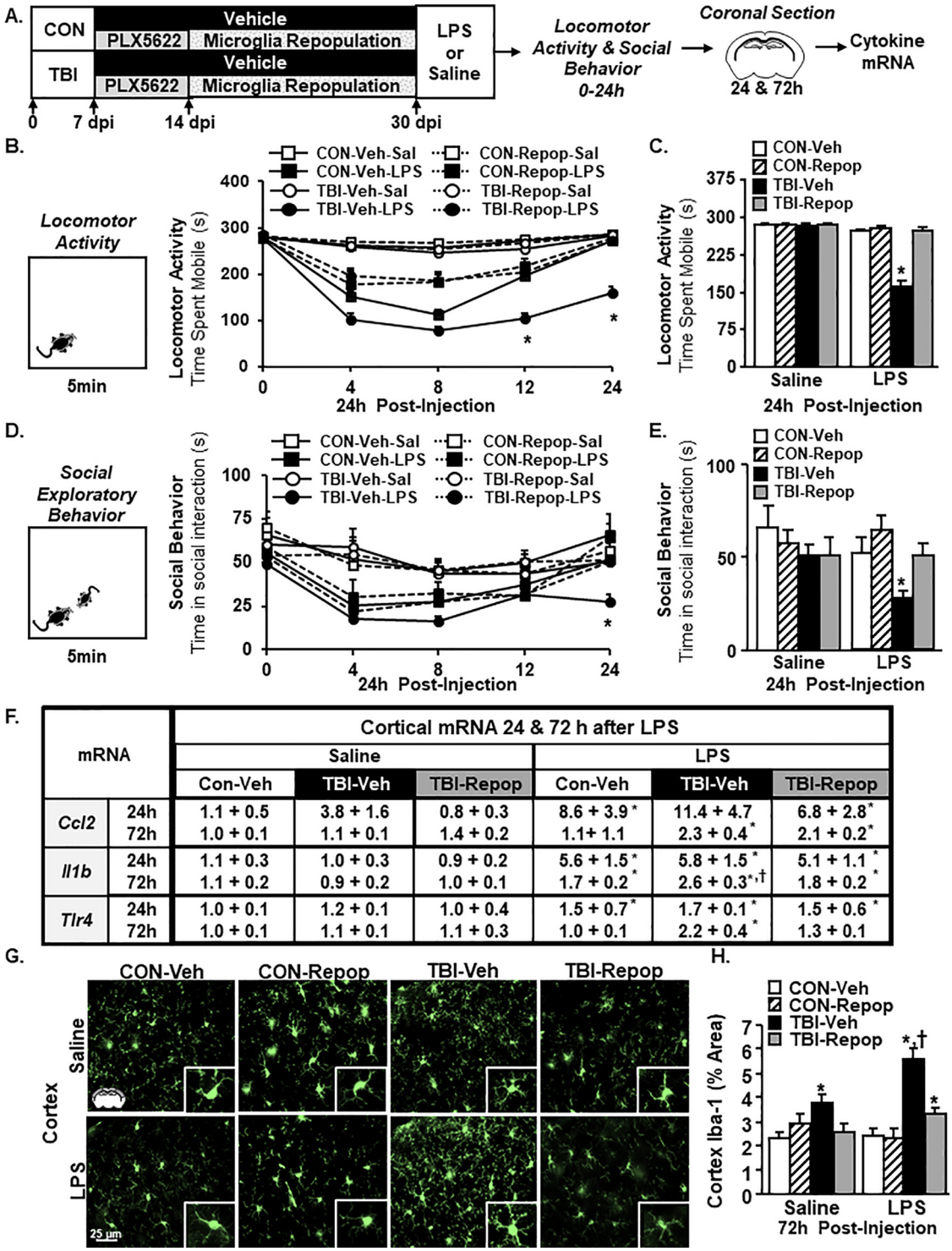

mRNA		Cortical mRNA 24 & 72 h after LPS					
		Saline			LPS		
		Con-Veh	TBI-Veh	TBI-Repop	Con-Veh	TBI-Veh	TBI-Repop
Ccl2	24h	1.1 + 0.5	3.8 + 1.6	0.8 + 0.3	8.6 + 3.9 *	11.4 + 4.7	6.8 + 2.8 *
	72h	1.0 + 0.1	1.1 + 0.1	1.4 + 0.2	1.1+ 1.1	2.3 + 0.4 *	2.1 + 0.2 *
Il1b	24h	1.1 + 0.3	1.0 + 0.3	0.9 + 0.2	5.6 + 1.5 *	5.8 + 1.5 *	5.1 + 1.1 *
	72h	1.1 + 0.2	0.9 + 0.2	1.0 + 0.1	1.7 + 0.2 *	2.6 + 0.3 *,†	1.8 + 0.2 *
Tlr4	24h	1.0 + 0.1	1.2 + 0.1	1.0 + 0.4	1.5 + 0.7 *	1.7 + 0.1 *	1.5 + 0.6 *
	72h	1.0 + 0.1	1.1 + 0.1	1.1 + 0.3	1.0 + 0.1	2.2 + 0.4 *	1.3 + 0.1

Figure 5. Immune reactivity 30 dpi was reduced by forced turnover of microglia. ***A***, Adult male C57BL/6 mice were subjected to mFPI (TBI) or left as uninjured controls. At 7 dpi, mice were provided diets formulated with either vehicle or a CSF1R antagonist (PLX5622) for 7d, and then returned to their standard rodent chow at 14 dpi. At 30 dpi (16 d of microglia repopulation), mice received an intraperitoneal injection of either saline or LPS (0.5 mg/kg) and locomotor activity and social exploratory behavior were assessed 0, 4, 8, 12, and 24 h later ($n = 9$). At 24 ($n = 6$) and 72 h ($n = 8$) after LPS, a coronal section was collected for mRNA analyses. ***B***, Time spent mobile in the open field over the 24-h time course. ***C***, Time spent mobile in the open field at 24 h postinjection. ***D***, Social exploratory behavior with a novel juvenile over the 24-h time course postinjection. ***E***, Social behavior with a novel juvenile at 24 h postinjection. ***F***, mRNA levels of *Ccl2*, *Il1b*, and *Tlr4* were determined in a coronal brain section 24 and 72 h postinjection. ***G***, Representative images of Iba-1$^+$ labeling in the cortex 72 h postinjection. ***H***, Percent area of Iba-1$^+$ microglia labeling in the cortex ($n = 5$). Bars represent mean ± SEM. Means with * are significantly different from CON-Veh ($p < 0.05$) and means with † are significantly different from both CON-Veh and PLX-Repop ($p < 0.05$).

Saline). For *Tlr4* mRNA at 72 h, the effect of LPS ($p < 0.04$) tended to be influenced by microglia turnover ($F_{(1,64)} = 2.3$, $p = 0.10$). *Post hoc* analysis indicates that the TBI-Veh-LPS group had the highest expression of *Tlr4* mRNA ($p < 0.05$) compared with all other groups including TBI-Repop-LPS and Con-Veh LPS groups at 72 h. Thus, there was prolonged (72 h) mRNA expression of *Tlr4* and *Il1b* in the cortex of TBI-Veh-LPS mice that was not present in either control LPS mice or TBI-LPS mice subjected to forced microglial turnover.

Another functional aspect of microglial reactivity is pronounced microglia restructuring after LPS injection (Fenn et al., 2014; Norden et al., 2015; Witcher et al., 2015). Therefore, Iba-1^+ labeling in the cortex was determined 72 h after LPS (Fig. 5*G*). The percent area of Iba-1^+ microglia in the cortex was increased by TBI ($F_{(1,40)} = 30.83$, $p < 0.001$; Fig. 5*H*). Moreover, the TBI-Veh-LPS mice had the highest Iba-1^+ percent area labeling in the cortex compared with all other groups ($p < 0.003$; Fig. 5*H*). Furthermore, Iba-1^+ labeling in TBI-Repop-LPS mice was reduced compared with TBI-Veh-LPS mice. Collectively, prolonged sickness behavior and increased microglial reactivity in TBI mice after LPS injection that was attenuated by the forced turnover of microglia.

Discussion

We aimed to determine whether forced microglial turnover 7 dpi improved recovery and reduced microglial priming 30 dpi. Evidence is provided that microglial turnover (7 d of PLX elimination, 16 d of repopulation; Fig. 2*A*) subacutely following diffuse TBI attenuated neuropathology associated mRNA expression in the cortex. Microglial turnover also reduced impaired neuronal connectivity and attenuated cognitive and behavioral complications 30 dpi. Furthermore, we show novel data that immune hyper-reactivity to LPS challenge 30 dpi was reduced with microglial turnover. Collectively, postinjury turnover of microglia mitigated functional deficits associated with diffuse TBI.

A key finding in this study was that microglia turnover reduced cortical neuropathology-associated mRNA profiles 30 dpi. mFPI causes diffuse axonal injury and inflammation throughout the neocortex, hippocampus, and thalamus (Bachstetter et al., 2013; Hylin et al., 2013). We selected 7 dpi to start turnover based on a robust IFN response and microglia priming in the cortex at this time (Witcher et al., 2021). This post-TBI turnover of microglia 7 dpi is an original design. Activation of IFN are relevant to neurotrauma (Abdullah et al., 2018; Sen et al., 2020; Todd et al., 2021) and promote "priming" of macrophages and microglia (Drokhlyansky et al., 2017; van der Poel et al., 2019) associated with increased mobilization, antigen processing and presentation, and debris clearance (Rawji et al., 2016). Here, there were 53 differentially expressed neuropathology genes in the cortex 30 dpi and a majority were restored by microglial turnover. Restored genes were primarily expressed by neurons (*Cck*, *Gria1*, *Nts*, *Slc17a6*) and astrocytes (*Aqp4*, *Gja1*, *Gfap*). Our interpretation is forced turnover of "trauma-associated microglia" containing robust IFN-related and priming associated mRNA profiles (Witcher et al., 2021) was critical for neuropathological resolution 30 dpi. These data expand our previous work showing that microglia elimination before TBI reduced inflammation and improved functional recovery (Witcher et al., 2021). Furthermore, these data are consistent with studies showing that microglial turnover in the chronic phase (30 dpi) of CCI, a penetrating brain injury, attenuated NOX2 and NLPR3 signaling (Henry et al., 2020). Another CCI study showed that microglia repopulation increased reparative profiles of microglia in the hippocampus (Willis et al., 2020). Here, specific microglia profiles were not determined, and the neuropathology panel was not focused on growth or repair-related genes. Thus, this warrants future studies. Collectively, post-TBI turnover of microglia improved the cortical microenvironment 30 dpi.

Related to the points above, our data with forced microglia turnover are unique in that mFPI was used to elicit a diffuse concussive injury, relevant to over 85% of clinical TBI (McKee and Daneshvar, 2015; Rowe et al., 2016). While penetrating TBI is relevant, it induces tissue cavitation, cell loss, and there is a robust contribution of peripheral leukocytes. Notably, mFPI does not have this extent of tissue damage or long-term infiltration of peripheral immune cells (Fenn et al., 2014; Witcher et al., 2018). Overall, demonstrating that microglial turnover-based interventions are effective in multiple types of TBI is significant and augments the field of neurotrauma.

Another important finding was that microglial turnover diminished behavioral and cognitive deficits 30 dpi. Depressive-like behavior 30 dpi was prevented by microglial turnover. Clinically, those who sustain TBI are at risk for depression and cognitive comorbidities (Jorge et al., 2004). Memory impairment in NOR/NOL tasks was detected 30 dpi, and these deficits were attenuated by microglial turnover. These results are consistent with myriad reports of cognitive impairments in mice post-TBI (Fenn et al., 2014; Muccigrosso et al., 2016; Witcher et al., 2021). These cognitive data are consistent with a report showing that microglial turnover initiated 30 d post-CCI attenuated cognitive decline (Henry et al., 2020). Overall, there was a microglia component to these behavioral and cognitive deficits 30 dpi that was reversed by microglial turnover.

We interpret the behavioral and cognitive data 30 dpi to indicate that inflammation and neuropathology meditated by microglia reduced neuronal plasticity. While TBI influenced dendritic remodeling, these changes were independent of microglial turnover. Increased MBP 30 dpi was unexpected, but may represent increased myelin debris. In fact, increased CSF and serum MBP are potential biomarkers of TBI in humans (Su et al., 2012; Wąsik et al., 2020). Because TBI-related changes in dendritic plasticity and MBP were unaffected by microglial turnover, this intervention did not reverse all TBI-induced neuropathology. Microglial turnover, however, was effective in improving neuronal connectivity 30 dpi by preventing reductions in both N1 and N2 components of action potentials. This is consistent with data that TBI modifies axons that project through cortical layers and into the corpus callosum (Ramos-Cejudo et al., 2018). Neuronal connectivity was reduced in the corpus callosum post-TBI (Reeves et al., 2016; Marion et al., 2018, 2019) and these deficits were microglia-dependent (Witcher et al., 2021). Here, TBI-induced reductions in connectivity were long-lasting (30 dpi) and there was a selective benefit of microglial turnover on neuronal connectivity compared with dendritic complexity and MBP content.

There was an effect of microglial turnover on cortical mRNA expression and N1 amplitude in controls. The mRNA profile alterations are consistent with data showing that microglia mRNA profiles were different 21 d after PLX-repopulation (Elmore et al., 2015). We used a 16-d repopulation paradigm to remove microglia 7 dpi and allow repopulation to evaluate recovery and immune reactivity 30 dpi. Thus, microglia profiles did not return to baseline expression and some genes were higher in

the cortex after repopulation compared with controls (Fig. 1*E*). There was also a difference in the N1 component of CAP in CON-Repop versus CON-Veh mice. The impact of this difference, however, was unclear. For example, compared with CON-Veh, repopulating microglia in controls had no effect on cortical spine volume or area, N2 amplitude, or cortical MBP. Moreover, microglia turnover did not affect baseline (control) assessments of motor function, cognition, or social behavior. While it is plausible that prolonged use of PLX5622 (or using transgenic CSFR1 mice) has negative side effects in the context of microglia interactions with neurons or endothelia (Delaney et al., 2021), there was no evidence of a significant confound here. Notably, mice were only exposed to PLX5622 for 7 d, which limits the potential confounds of this CSFR1 antagonist. Thus, the removal of the trauma-associated and primed microglia outweighed the general effects of repopulation.

A key finding was that microglial turnover attenuated immune reactivity of TBI mice 30 dpi. For example, microglial priming was associated with an exaggerated inflammatory response to an immune challenge with protracted lethargy, social withdrawal and depressive-like behavior (Fenn et al., 2014; Muccigrosso et al., 2016). Our previous data at 7 dpi point to IFN responses as key mediators for priming microglia (Witcher et al., 2021). This is consistent with other studies showing IFN responds to tissue damage and is an alarm system for microglia (Prinz and Knobeloch, 2012; Barrett et al., 2020). Remnants of IFN and inflammatory responses remained elevated in the cortex 30 dpi based on neuropathology mRNA analyses. This functional priming of microglia is predicted to increase cytokine responses to subsequent CNS injuries, stressors, and immune challenges (Witcher et al., 2015; Kokiko-Cochran and Godbout, 2018). Notably, most TBI survivors do not experience repeated injuries throughout life, but will experience multiple infections (Kourbeti et al., 2012). LPS-induced lethargy and social withdrawal were extended in TBI-Veh-LPS mice compared with all other groups (Fenn et al., 2014). The advancement of this study was that these LPS-associated behavioral deficits 30 dpi were prevented by microglial turnover. In terms of an exaggerated immune response, the LPS-induced cytokine mRNA expression in the brain was not influenced by TBI until 72 h after challenge. It is unclear why the cytokine mRNA data 24 h was less consistent with previous studies (Fenn et al., 2014). One explanation is that mRNA expression in coronal brain sections was determined as opposed to in isolated microglia. Nonetheless, *Il1ß* and *Tlr4* mRNA were highest in TBI-Veh-LPS groups at 72 h. Moreover, there was increased structural reactivity of cortical microglia 72 h post-LPS in the TBI-Veh-LPS group that was attenuated by turnover. While there are more parameters to investigate concerning TBI and immune reactivity, forced microglial turnover attenuated several components of the TBI-associated immune reactivity to LPS.

CSF1R antagonism will affect other long-lived tissue macrophages in the brain and periphery (Lee et al., 2018; Lei et al., 2020). Here, there were no differences in monocytes, granulocytes, B-cells, and T-cells in bone marrow or the spleen 30 dpi with this forced microglia turnover paradigm. Our previous study showed no effect on monocyte numbers in circulation after a similar turnover protocol (Weber et al., 2019). Because these myeloid cells return to baseline levels, this turnover design has some potential advantages. For example, the profile of these myeloid cells may be different with repopulation, which may be beneficial in the context of inflammation and immune priming.

In summary, microglial turnover 7 d following TBI alleviated functional impairments associated with microglial priming and immune reactivity 30 dpi. Therefore, microglia represent a therapeutic target after TBI to reduce persistent neuropathological processes and improve recovery.

References

Abdullah A, Zhang M, Frugier T, Bedoui S, Taylor JM, Crack PJ (2018) STING-mediated type-I interferons contribute to the neuroinflammatory process and detrimental effects following traumatic brain injury. J Neuroinflammation 15:323.

Antunes M, Biala G (2012) The novel object recognition memory: neurobiology, test procedure, and its modifications. Cogn Process 13:93–110.

Bachstetter AD, Rowe RK, Kaneko M, Goulding D, Lifshitz J, Van Eldik LJ (2013) The p38alpha MAPK regulates microglial responsiveness to diffuse traumatic brain injury. J Neurosci 33:6143–6153.

Bachstetter AD, Van Eldik LJ, Schmitt FA, Neltner JH, Ighodaro ET, Webster SJ, Patel E, Abner EL, Kryscio RJ, Nelson PT (2015) Disease-related microglia heterogeneity in the hippocampus of Alzheimer's disease, dementia with Lewy bodies, and hippocampal sclerosis of aging. Acta Neuropathol Commun 3:32.

Barrett JP, Henry RJ, Shirey KA, Doran SJ, Makarevich OD, Ritzel RM, Meadows VA, Vogel SN, Faden AI, Stoica BA, Loane DJ (2020) Interferon-beta plays a detrimental role in experimental traumatic brain injury by enhancing neuroinflammation that drives chronic neurodegeneration. J Neurosci 40:2357–2370.

Brooks WM, Stidley CA, Petropoulos H, Jung RE, Weers DC, Friedman SD, Barlow MA, Sibbitt WL, Yeo RA (2000) Metabolic and cognitive response to human traumatic brain injury: a quantitative proton magnetic resonance study. J Neurotrauma 17:629–640.

Corona AW, Norden DM, Skendelas JP, Huang Y, O'Connor JC, Lawson M, Dantzer R, Kelley KW, Godbout JP (2013) Indoleamine 2,3-dioxygenase inhibition attenuates lipopolysaccharide induced persistent microglial activation and depressive-like complications in fractalkine receptor (CX (3)CR1)-deficient mice. Brain Behav Immun 31:134–142.

Coughlin JM, Wang Y, Munro CA, Ma S, Yue C, Chen S, Airan R, Kim PK, Adams AV, Garcia C, Higgs C, Sair HI, Sawa A, Smith G, Lyketsos CG, Caffo B, Kassiou M, Guilarte TR, Pomper MG (2015) Neuroinflammation and brain atrophy in former NFL players: an in vivo multimodal imaging pilot study. Neurobiol Dis 74:58–65.

Coughlin JM, et al. (2017) Imaging of glial cell activation and white matter integrity in brains of active and recently retired national football league players. JAMA Neurol 74:67–74.

Delaney C, Farrell M, Doherty CP, Brennan K, O'Keeffe E, Greene C, Byrne K, Kelly E, Birmingham N, Hickey P, Cronin S, Savvides SN, Doyle SL, Campbell M (2021) Attenuated CSF-1R signalling drives cerebrovascular pathology. EMBO Mol Med 13:e12889.

Denninger JK, Smith BM, Kirby ED (2018) Novel object recognition and object location behavioral testing in mice on a budget. J Vis Exp. doi:10.3791/58593.

Drokhlyansky E, Goz Ayturk D, Soh TK, Chrenek R, O'Loughlin E, Madore C, Butovsky O, Cepko CL (2017) The brain parenchyma has a type I interferon response that can limit virus spread. Proc Natl Acad Sci U S A 114:E95–E104.

Elmore MR, Najafi AR, Koike MA, Dagher NN, Spangenberg EE, Rice RA, Kitazawa M, Matusow B, Nguyen H, West BL, Green KN (2014) Colony-stimulating factor 1 receptor signaling is necessary for microglia viability, unmasking a microglia progenitor cell in the adult brain. Neuron 82:380–397.

Elmore MR, Lee RJ, West BL, Green KN (2015) Characterizing newly repopulated microglia in the adult mouse: impacts on animal behavior, cell morphology, and neuroinflammation. PLoS One 10:e0122912.

Erion JR, Wosiski-Kuhn M, Dey A, Hao S, Davis CL, Pollock NK, Stranahan AM (2014) Obesity elicits interleukin 1-mediated deficits in hippocampal synaptic plasticity. J Neurosci 34:2618–2631.

Faul M, Coronado V (2015) Epidemiology of traumatic brain injury. Handb Clin Neurol 127:3–13.

Fenn AM, Gensel JC, Huang Y, Popovich PG, Lifshitz J, Godbout JP (2014) Immune activation promotes depression 1 month after diffuse brain injury: a role for primed microglia. Biol Psychiatry 76:575–584.

Fenn AM, Skendelas JP, Moussa DN, Muccigrosso MM, Popovich PG, Lifshitz J, Eiferman DS, Godbout JP (2015) Methylene blue attenuates traumatic brain injury-associated neuroinflammation and acute depressive-like behavior in mice. J Neurotrauma 32:127–138.

Fleminger S (2008) Long-term psychiatric disorders after traumatic brain injury. Eur J Anaesthesiol Suppl 42:123–130.

Hao S, Dey A, Yu X, Stranahan AM (2016) Dietary obesity reversibly induces synaptic stripping by microglia and impairs hippocampal plasticity. Brain Behav Immun 51:230–239.

Henry RJ, Ritzel RM, Barrett JP, Doran SJ, Jiao Y, Leach JB, Szeto GL, Wu J, Stoica BA, Faden AI, Loane DJ (2020) Microglial depletion with CSF1R inhibitor during chronic phase of experimental traumatic brain injury reduces neurodegeneration and neurological deficits. J Neurosci 40:2960–2974.

Himanen L, Portin R, Isoniemi H, Helenius H, Kurki T, Tenovuo O (2006) Longitudinal cognitive changes in traumatic brain injury: a 30-year follow-up study. Neurology 66:187–192.

Huang Y, Xu Z, Xiong S, Qin G, Sun F, Yang J, Yuan TF, Zhao L, Wang K, Liang YX, Fu L, Wu T, So KF, Rao Y, Peng B (2018) Dual extra-retinal origins of microglia in the model of retinal microglia repopulation. Cell Discov 4:9.

Hylin MJ, Orsi SA, Zhao J, Bockhorst K, Perez A, Moore AN, Dash PK (2013) Behavioral and histopathological alterations resulting from mild fluid percussion injury. J Neurotrauma 30:702–715.

Jackson JC, Gordon SM, Hart RP, Hopkins RO, Ely EW (2004) The association between delirium and cognitive decline: a review of the empirical literature. Neuropsychol Rev 14:87–98.

Johnson VE, Stewart JE, Begbie FD, Trojanowski JQ, Smith DH, Stewart W (2013) Inflammation and white matter degeneration persist for years after a single traumatic brain injury. Brain 136:28–42.

Jorge RE, Robinson RG, Moser D, Tateno A, Crespo-Facorro B, Arndt S (2004) Major depression following traumatic brain injury. Arch Gen Psychiatry 61:42–50.

Kelley BJ, Lifshitz J, Povlishock JT (2007) Neuroinflammatory responses after experimental diffuse traumatic brain injury. J Neuropathol Exp Neurol 66:989–1001.

Kokiko-Cochran ON, Godbout JP (2018) The inflammatory continuum of traumatic brain injury and Alzheimer's disease. Front Immunol 9:672.

Kourbeti IS, Vakis AF, Papadakis JA, Karabetsos DA, Bertsias G, Filippou M, Ioannou A, Neophytou C, Anastasaki M, Samonis G (2012) Infections in traumatic brain injury patients. Clin Microbiol Infect 18:359–364.

Lee S, Shi XQ, Fan A, West B, Zhang J (2018) Targeting macrophage and microglia activation with colony stimulating factor 1 receptor inhibitor is an effective strategy to treat injury-triggered neuropathic pain. Mol Pain 14:1744806918764979.

Lei F, Cui N, Zhou C, Chodosh J, Vavvas DG, Paschalis EI (2020) CSF1R inhibition by a small-molecule inhibitor is not microglia specific; affecting hematopoiesis and the function of macrophages. Proc Natl Acad Sci U S A 117:23336–23338.

Lifshitz J, Kelley BJ, Povlishock JT (2007) Perisomatic thalamic axotomy after diffuse traumatic brain injury is associated with atrophy rather than cell death. J Neuropathol Exp Neurol 66:218–229.

Lifshitz J, Rowe RK, Griffiths DR, Evilsizor MN, Thomas TC, Adelson PD, McIntosh TK (2016) Clinical relevance of midline fluid percussion brain injury: acute deficits, chronic morbidities and the utility of biomarkers. Brain Inj 30:1293–1301.

Loane DJ, Kumar A, Stoica BA, Cabatbat R, Faden AI (2014) Progressive neurodegeneration after experimental brain trauma: association with chronic microglial activation. J Neuropathol Exp Neurol 73:14–29.

Love MI, Huber W, Anders S (2014) Moderated estimation of fold change and dispersion for RNA-seq data with DESeq2. Genome Biol 15:550.

Marion CM, Radomski KL, Cramer NP, Galdzicki Z, Armstrong RC (2018) Experimental traumatic brain injury identifies distinct early and late phase axonal conduction deficits of white matter pathophysiology, and reveals intervening recovery. J Neurosci 38:8723–8736.

Marion CM, McDaniel DP, Armstrong RC (2019) Sarm1 deletion reduces axon damage, demyelination, and white matter atrophy after experimental traumatic brain injury. Exp Neurol 321:113040.

McKee AC, Daneshvar DH (2015) The neuropathology of traumatic brain injury. Handb Clin Neurol 127:45–66.

McKim DB, Niraula A, Tarr AJ, Wohleb ES, Sheridan JF, Godbout JP (2016) Neuroinflammatory dynamics underlie memory impairments after repeated social defeat. J Neurosci 36:2590–2604.

McKim DB, Weber MD, Niraula A, Sawicki CM, Liu X, Jarrett BL, Ramirez-Chan K, Wang Y, Roeth RM, Sucaldito AD, Sobol CG, Quan N, Sheridan JF, Godbout JP (2018) Microglial recruitment of IL-1β-producing monocytes to brain endothelium causes stress-induced anxiety. Mol Psychiatry 23:1421–1431.

Mouzon BC, Bachmeier C, Ferro A, Ojo JO, Crynen G, Acker CM, Davies P, Mullan M, Stewart W, Crawford F (2014) Chronic neuropathological and neurobehavioral changes in a repetitive mild traumatic brain injury model. Ann Neurol 75:241–254.

Muccigrosso MM, Ford J, Benner B, Moussa D, Burnsides C, Fenn AM, Popovich PG, Lifshitz J, Walker FR, Eiferman DS, Godbout JP (2016) Cognitive deficits develop 1 month after diffuse brain injury and are exaggerated by microglia-associated reactivity to peripheral immune challenge. Brain Behav Immun 54:95–109.

Najafi AR, Crapser J, Jiang S, Ng W, Mortazavi A, West BL, Green KN (2018) A limited capacity for microglial repopulation in the adult brain. Glia 66:2385–2396.

Norden DM, Fenn AM, Dugan A, Godbout JP (2014) TGFbeta produced by IL-10 redirected astrocytes attenuates microglial activation. Glia 62:881–895.

Norden DM, Muccigrosso MM, Godbout JP (2015) Microglial priming and enhanced reactivity to secondary insult in aging, and traumatic CNS injury, and neurodegenerative disease. Neuropharmacology 96:29–41.

O'Neil SM, Witcher KG, McKim DB, Godbout JP (2018) Forced turnover of aged microglia induces an intermediate phenotype but does not rebalance CNS environmental cues driving priming to immune challenge. Acta Neuropathol Commun 6:129.

Prinz M, Knobeloch KP (2012) Type I interferons as ambiguous modulators of chronic inflammation in the central nervous system. Front Immunol 3:67.

Ramlackhansingh AF, Brooks DJ, Greenwood RJ, Bose SK, Turkheimer FE, Kinnunen KM, Gentleman S, Heckemann RA, Gunanayagam K, Gelosa G, Sharp DJ (2011) Inflammation after trauma: microglial activation and traumatic brain injury. Ann Neurol 70:374–383.

Ramos RL, Tam DM, Brumberg JC (2008) Physiology and morphology of callosal projection neurons in mouse. Neuroscience 153:654–663.

Ramos-Cejudo J, Wisniewski T, Marmar C, Zetterberg H, Blennow K, de Leon MJ, Fossati S (2018) Traumatic brain injury and Alzheimer's disease: the cerebrovascular link. EBioMedicine 28:21–30.

Rawji KS, Mishra MK, Michaels NJ, Rivest S, Stys PK, Yong VW (2016) Immunosenescence of microglia and macrophages: impact on the ageing central nervous system. Brain 139:653–661.

Reeves TM, Trimmer PA, Colley BS, Phillips LL (2016) Targeting Kv1.3 channels to reduce white matter pathology after traumatic brain injury. Exp Neurol 283:188–203.

Rowe RK, Griffiths DR, Lifshitz J (2016) Midline (central) fluid percussion model of traumatic brain injury. Methods Mol Biol 1462:211–230.

Schaffert J, LoBue C, White CL, Chiang HS, Didehbani N, Lacritz L, Rossetti H, Dieppa M, Hart J, Cullum CM (2018) Traumatic brain injury history is associated with an earlier age of dementia onset in autopsy-confirmed Alzheimer's disease. Neuropsychology 32:410–416.

Sen T, Saha P, Gupta R, Foley LM, Jiang T, Abakumova OS, Hitchens TK, Sen N (2020) Aberrant ER stress induced neuronal-IFNbeta elicits white matter injury due to microglial activation and T-cell infiltration after TBI. J Neurosci 40:424–446.

Silver JM, McAllister TW, Arciniegas DB (2009) Depression and cognitive complaints following mild traumatic brain injury. Am J Psychiatry 166:653–661.

Su E, Bell MJ, Kochanek PM, Wisniewski SR, Bayir H, Clark RS, Adelson PD, Tyler-Kabara EC, Janesko-Feldman KL, Berger RP (2012) Increased CSF concentrations of myelin basic protein after TBI in infants and children: absence of significant effect of therapeutic hypothermia. Neurocrit Care 17:401–407.

Till C, Colella B, Verwegen J, Green RE (2008) Postrecovery cognitive decline in adults with traumatic brain injury. Arch Phys Med Rehabil 89:S25–S34.

Todd BP, Chimenti MS, Luo Z, Ferguson PJ, Bassuk AG, Newell EA (2021) Traumatic brain injury results in unique microglial and

astrocyte transcriptomes enriched for type I interferon response. J Neuroinflammation 18:151.

van der Poel M, Ulas T, Mizee MR, Hsiao CC, Miedema SSM, Schuurman A, KG, Helder B, Tas SW, Schultze JL, Hamann J, Huitinga I (2019) Transcriptional profiling of human microglia reveals grey-white matter heterogeneity and multiple sclerosis-associated changes. Nat Commun 10:1139.

van Tilborg E, van Kammen CM, de Theije CGM, van Meer MPA, Dijkhuizen RM, Nijboer CH (2017) A quantitative method for microstructural analysis of myelinated axons in the injured rodent brain. Sci Rep 7:16492.

Wang HK, Lin SH, Sung PS, Wu MH, Hung KW, Wang LC, Huang CY, Lu K, Chen HJ, Tsai KJ (2012) Population based study on patients with traumatic brain injury suggests increased risk of dementia. J Neurol Neurosurg Psychiatry 83:1080–1085.

Wąsik N, Sokół B, Hołysz M, Mańko W, Juszkat R, Jagodziński PP, Jankowski R (2020) Serum myelin basic protein as a marker of brain injury in aneurysmal subarachnoid haemorrhage. Acta Neurochir 162:545–552.

Weber MD, McKim DB, Niraula A, Witcher KG, Yin W, Sobol CG, Wang Y, Sawicki CM, Sheridan JF, Godbout JP (2019) The influence of microglial elimination and repopulation on stress sensitization induced by repeated social defeat. Biol Psychiatry 85:667–678.

Willis EF, MacDonald KPA, Nguyen QH, Garrido AL, Gillespie ER, Harley SBR, Bartlett PF, Schroder WA, Yates AG, Anthony DC, Rose-John S, Ruitenberg MJ, Vukovic J (2020) Repopulating microglia promote brain repair in an IL-6-dependent manner. Cell 180:833–846.e16.

Witcher KG, Eiferman DS, Godbout JP (2015) Priming the inflammatory pump of the CNS after traumatic brain injury. Trends Neurosci 38:609–620.

Witcher KG, Bray CE, Dziabis JE, McKim DB, Benner BN, Rowe RK, Kokiko-Cochran ON, Popovich PG, Lifshitz J, Eiferman DS, Godbout JP (2018) Traumatic brain injury-induced neuronal damage in the somatosensory cortex causes formation of rod-shaped microglia that promote astrogliosis and persistent neuroinflammation. Glia 66:2719–2736.

Witcher KG, Bray CE, Chunchai T, Zhao F, O'Neil SM, Gordillo AJ, Campbell WA, McKim DB, Liu X, Dziabis JE, Quan N, Eiferman DS, Fischer AJ, Kokiko-Cochran ON, Askwith C, Godbout JP (2020) Traumatic brain injury causes chronic cortical inflammation and neuronal dysfunction mediated by microglia. J Neurosci 41:1597–1616.

Witcher KG, Bray CE, Chunchai T, Zhao F, O'Neil SM, Gordillo AJ, Campbell WA, McKim DB, Liu X, Dziabis JE, Quan N, Eiferman DS, Fischer AJ, Kokiko-Cochran ON, Askwith C, Godbout JP (2021) Traumatic brain injury causes chronic cortical inflammation and neuronal dysfunction mediated by microglia. J Neurosci 41:1597–1616.

Wohleb ES, Hanke ML, Corona AW, Powell ND, Stiner LM, Bailey MT, Nelson RJ, Godbout JP, Sheridan JF (2011) β-Adrenergic receptor antagonism prevents anxiety-like behavior and microglial reactivity induced by repeated social defeat. J Neurosci 31:6277–6288.

Wohleb ES, Fenn AM, Pacenta AM, Powell ND, Sheridan JF, Godbout JP (2012) Peripheral innate immune challenge exaggerated microglia activation, increased the number of inflammatory CNS macrophages, and prolonged social withdrawal in socially defeated mice. Psychoneuroendocrinology 37:1491–1505.

Wohleb ES, Powell ND, Godbout JP, Sheridan JF (2013) Stress-induced recruitment of bone marrow-derived monocytes to the brain promotes anxiety-like behavior. J Neurosci 33:13820–13833.

Wohleb ES, McKim DB, Shea DT, Powell ND, Tarr AJ, Sheridan JF, Godbout JP (2014) Re-establishment of anxiety in stress-sensitized mice is caused by monocyte trafficking from the spleen to the brain. Biol Psychiatry 75:970–981.

Wynne AM, Henry CJ, Godbout JP (2009) Immune and behavioral consequences of microglial reactivity in the aged brain. Integr Comp Biol 49:254–266.

Zhan L, Krabbe G, Du F, Jones I, Reichert MC, Telpoukhovskaia M, Kodama L, Wang C, Cho S-H, Sayed F, Li Y, Le D, Zhou Y, Shen Y, West B, Gan L (2019) Proximal recolonization by self-renewing microglia re-establishes microglial homeostasis in the adult mouse brain. PLoS Biol 17: e3000134.